JOURNAL OF Applied Polymer SCIENCE

Effects of short fiber tip geometry and inhomogeneous interphase on the stress distribution of rubber matrix sealing composites

Xiaoming Yu, Boqin Gu, Bin Zhang
School of Mechanical and Power Engineering, Nanjing Tech University, Nanjing, People's Republic of China
Correspondence to: B. Gu (E-mail: bqgu@njtech.edu.cn)

ABSTRACT: The normal and interfacial shear stress distributions with flat fiber tip of short-fiber-reinforced rubber matrix sealing composites (SFRC) compared with the shear lag model were investigated by using the finite element method (FEM). The results indicate that stress values do not agree with those calculated by the shear lag model. The effect of different geometrical shapes of fiber tip on the stress distributions of SFRC was also investigated. The geometrical shapes of fiber tip under present investigation are flat, semi-elliptical, hemispherical, and circular cone, respectively. The results show that the hemispherical fiber tip transfers the load with less stress concentration and is contributed to controlling the interface debonding failure more effectively than other shapes of fiber tip. Further study on the effect of the inhomogeneous interphase properties on the normal and interfacial shear stresses of hemispherical fiber tip was also conducted. The results indicate that the normal stress increases with the increase of the interphase thickness and interfacial shear stress remains unchanged, and the normal stress values of SFRC with interphase are higher than those without interphase. The interphase elastic modulus has no influence on the stress distributions along the direction to the fiber axis. The stress distributions along the radial direction in the interphase end are largely dependent on the interphase elastic modulus, and the interfacial shear stress is larger than the normal stress, which reveals that a significant part of the external load is transferred from the fiber to the matrix through shear stresses within the interphase. © 2014 Wiley Periodicals, Inc. J. Appl. Polym. Sci. **2015**, *132*, 41638.

KEYWORDS: composites; fibers; theory and modeling; rubber; surfaces and interfaces

Received 6 July 2014; accepted 12 October 2014
DOI: 10.1002/app.41638

INTRODUCTION

Short-fiber-reinforced rubber matrix sealing composites (SFRC), such as aramid, glass, and carbon fibers reinforced rubber sheet, etc., are widely used in petroleum, chemical, textile, electrical, and mechanical industry. Fibers or particles embedded in a rubber matrix can effectively improve the comprehensive performance of materials, for example high strength, fatigue resistance, corrosion resistance, etc. Engineering practice confirms that this kind of SFRC has good applicability over recent years.[1,2] The performance of the composites was predicted by an amount of existing theoretical models.[3,4] Cox model is one of the most popular models because it is widely used to calculate deformational and elastic properties of discontinuous fibers in fiber-reinforced composites.[5] The accuracy of the model is largely dependent on the imposed boundary conditions at the fiber ends. Generally, stress boundary conditions, based on arbitrary assumptions, are predefined at the fibers ends to obtain analytical solutions from the governing equations.[6] However, Hsueh[7] pointed out these stresses cannot be predetermined, and therefore, the boundary conditions are ambiguous. Hsueh[7] as well as Nair and Kim[8] proposed a new model to acquire analytical solutions of the stress at the fiber ends by using the methods of fictitious fibers (made of matrix material). The performance of composites such as fiber reinforced resin matrix, metal matrix, etc.[9,10] can be accurately predicted by the traditional and improved theoretical models. However, the prediction of stress transfer by the above theoretical models produces a larger error for fiber elastic modulus is usually much greater than that of the matrix. The elastic modulus ratio of fiber and matrix of SFRC is more than 1000. Therefore, it is necessary to further strengthen the research work of SFRC so as to achieve the purpose of optimizing mesoscopic structure of materials and improving the overall mechanical properties of materials by setting up the relationship between mesoscopic structure and macro mechanical properties.

A number of studies have been done on understanding the micromechanical behavior of short-fiber-reinforced composites. Jacob *et al.*[11] investigated the viscoelastic properties of the woven sisal fabric reinforced natural rubber composites. The results showed that the storage modulus was found to increase upon reinforcement of the natural rubber with sisal fabric. Coffey *et al.*[12] investigated the interfacial micromechanics of aramid fibers with flat

fiber tip in an engineering thermoplastic elastomer by determining the stress distributions along fibers in an single-fiber model composites using Raman spectroscopy. In Lee's recent research,[13] fiber length distribution and fiber orientation in fiber reinforced composites were studied, which were regarded as important factors to determine mechanical properties of the composites.

At present, though the research on the influence of the fiber mesoscopic parameters on the macroperformance of composites have made a certain progress based on the shear lag model, the self-consistent theory, and equivalent inclusion theory, there are too many simplifications and approximations in theoretical analysis model, and the research is not very perfect. Besides, Raman spectroscopy[14,15] offers an experimental method with acceptable resolution for the study of stress distribution near loaded fibers. The experimental results show large scattering in the measured normal stress values along the fiber length, perhaps due to the, respectively, large diameter of the laser beam, which is of the order of 2 μm.[16] Stress values vary abruptly in the interface region. Thus, the accurate estimation of the stress field is quite difficult to achieve by experimental methods. Finite element analysis method based on the real fiber geometry may be an effective way to study such issues at mesoscopic level, and the relevant research is still rare up to now.

Two-phase materials have been exploited for decades in engineering design, and they have been proved having great applicability and high performance. However, it has been suggested that some materials previously considered to be two-phase composites are better described in terms of a third phase.[17,18] Interphase performance was considered as a key factor in the study of comprehensive mechanical performance of composites. Zhang and Gu[19] studied the effect of thickness and elastic modulus of interphase on the properties of short fiber reinforced composite materials. Yuan *et al.*[20] established finite element method (FEM) model of interfacial reaction layer and analyzed the influence of interface reaction on interfacial shear strength of the composites.

While an interphase typically accounts for less than 2% of the total mass of the material in composites, it has been shown that longitudinal tensile strength is improved by as much as 29%, compressive strength by as much as 50% and notched fatigue lifetime cycles by as many as two orders of magnitude.[21]

Fibers are typically 5–12 μm in diameter and an interphase region can be of the order of 0.2 μm. However, definitive verification of the interface thickness is not usually possible.[22] Kim *et al.*[23] measured the interphase thickness in a glass epoxy composite, by means of three different experimental techniques, namely, nanoindentation, nanoscratch, and differential scanning calorimetry tests, respectively. The results showed three different values of the interphase thickness, for the same material. Shen and Li[24] presented the selection of interphase performance of short fiber reinforced composites. In many publications,[25–27] the performances of interphase are not constants, but vary with the thickness of the interphase.

Based on the single fiber axisymmetrical of an aligned SFRC with the flat tip, the normal and interfacial shear stress distributions along the fiber length and near the tip were investigated by FEM, and the results obtained by simulation were compared with those by shear lag model. The effect of the shapes of the fiber tip and the performance of inhomogeneous interphase on stress distributions were researched both by simulation and shear lag model, and the optimum shapes of fiber tip were also determined.

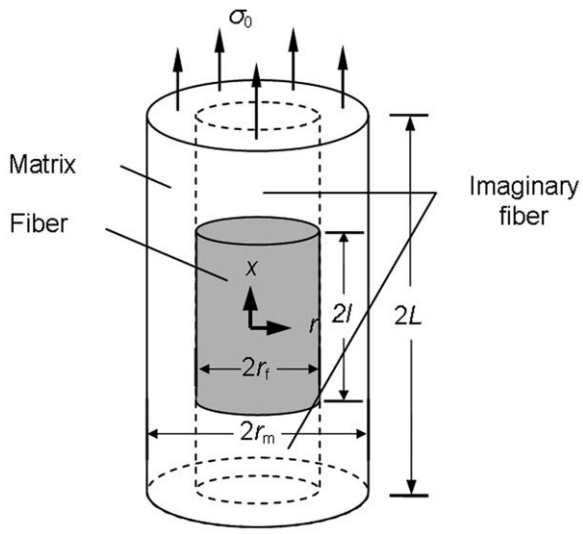

Figure 1. Model geometry and coordinate system.

THE STRESS EXPRESSIONS ACCORDING TO THE IMPROVED THE SHEAR LAG MODEL

The shear lag model is widely used to calculate deformational and elastic properties of discontinuous fibers in fiber reinforced composites.[17] Representative volume element (RVE) can be described in terms of two-dimensional cylindrical coordinates (r, x), as shown in Figure 1. It is composed of a cylindrical matrix of length $2L$ and radius r_m, containing a cylindrical fiber with length $2l$ and radius r_f. Fibers and matrix are coaxial. The dashed part in the matrix is imaginary fiber; RVE is subject to an uniform tensile stress σ_0 at the ends, where only the matrix is present. The applied stress is parallel to the fiber axis, and no sliding is allowed between the matrix and fiber at the interface $r = r_f$. The equations describing the normal and shear stresses in the interphase between the fiber and matrix can be written as

$$\sigma_f(x) = \frac{r_f^2 E_f \sigma_0}{S} + 2A\cosh(\beta x) \tag{1}$$

$$\tau_f(r_f, x) = -r_f \beta A \sinh(\beta x) \tag{2}$$

where S, A, and β are given in eqs. (3–6).

$$S = r_f^2 E_f + \left(r_m^2 - r_f^2\right) E_m \tag{3}$$

$$\beta = \sqrt{\frac{SH}{r_m^2 E_f}} \tag{4}$$

$$H = \frac{r_m^2}{r_f^2(1+\nu_m)\left[r_m^2 \ln(r_m/r_f) - \frac{r_m^2 - r_f^2}{2}\right]} \tag{5}$$

$$A = \frac{\sigma_0\left(r_m^2 - r_f^2\right)(E_m - E_f)}{S\left\langle 2\cosh(\beta l) - \frac{\beta\left\{2\sinh(\beta l)\left[\exp\left(\sqrt{H}l\right) - \exp\left[\sqrt{H}(2L-l)\right]\right]\right\}}{\sqrt{H}\left\{\exp\left(\sqrt{H}l\right) + \exp\left[\sqrt{H}(2L-l)\right]\right\}}\right\rangle} \tag{6}$$

where E_f and E_m are elastic moduli of fiber and matrix, respectively.

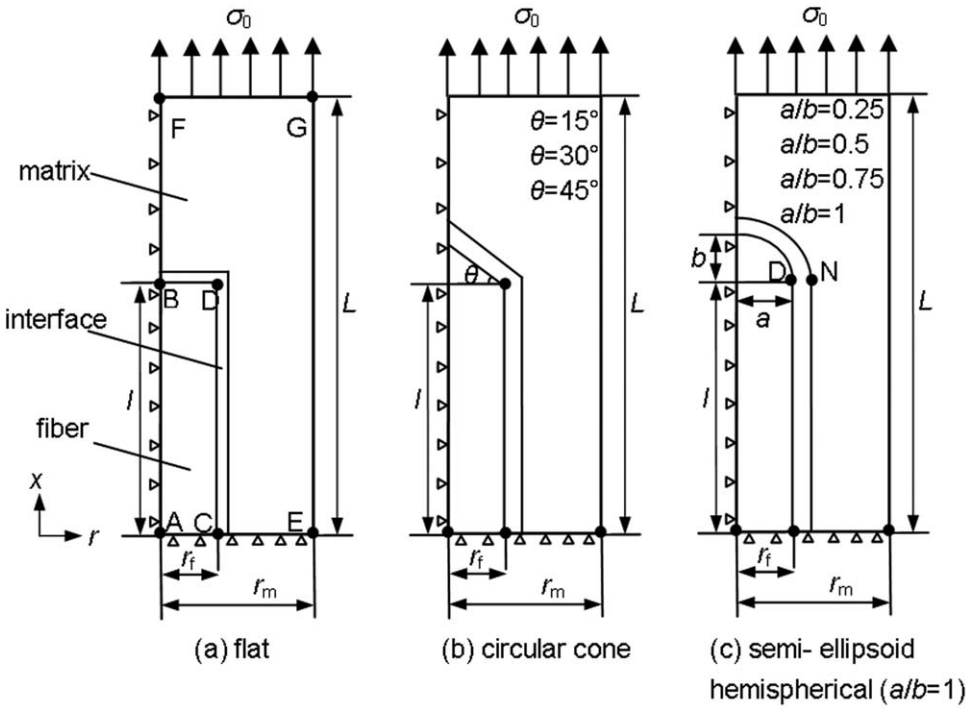

Figure 2. Shapes and dimension of the fiber tip.

The equations describing the normal and shear stresses in the interphase between the imaginary fiber and matrix can be written as

$$\sigma_{\mathrm{ff}}(x)=\exp\left(\sqrt{H}x\right)c_1+\exp\left(-\sqrt{H}x\right)c_2+\sigma_0 \tag{7}$$

$$\tau_{\mathrm{ff}}(r_f,x)=-\frac{r_f\sqrt{H}}{2}\left[\exp\left(\sqrt{H}x\right)c_1-\exp\left(-\sqrt{H}x\right)c_2\right] \tag{8}$$

where c_1 and c_2 are given in eqs. (9) and (10).

$$c_1=\frac{2\beta A\sinh(\beta l)}{\sqrt{H}\left\{\exp\left(\sqrt{H}l\right)+\exp\left[\sqrt{H}(2L-l)\right]\right\}} \tag{9}$$

$$c_2=-c_1\exp\left(2\sqrt{H}L\right) \tag{10}$$

CONTENT AND METHOD OF NUMERICAL SIMULATION

The main concern of present investigation is the interfacial shear stress and normal stress distributions of SFRC along the direction to the fiber axis by FEM. The material under present investigation is an aramid/rubber composite with material properties are as follows: Young's modulus and Poisson ratio of the fiber are $E_f=136$ GPa and $\nu_f=0.2$, respectively; Young's modulus and Poisson ratio of the matrix are $E_m=128$ MPa and $\nu_m=0.3$, separately.[12]

Some simplifying assumptions must be made regarding the material properties of constituent elements of SFRC. The assumptions used are: (a) Fibers are unidirectional, continuous, and uniformly spaced. (b) Fiber and matrix behave in a linearly elastic manner. (c) Fiber and matrix are homogeneous isotropic. (d) Composite behavior can be modeled by a RVE.

In order to investigate the effect of the shapes of the fiber tip on the stress distribution, four kinds of geometrical shapes of fiber tips were taken into consideration, and they are flat, circular cone, hemispherical, and semi-ellipsoid, respectively, as shown in Figure 2. It is assumed that the fiber has constant radius $r_f=6$ μm and ratio of the fiber length to diameter, $l/r_f=5$. The matrix has constant radius $r_m=5r_f$ and half-length $L=l+10r_f$. The physical model is assumed consisting of a fiber surrounded by matrix and subjected to a uniform tension parallel to the fiber direction. Only one quarter of the actual physical model is required in the analysis due to the axisymmetric symmetry.

Load and boundary conditions are as shown in Figure 2. The RVE is loaded on line FG with a tensile stress σ_0. For the present finite element model, the boundary conditions are given as follows:

$$u_r=0 \quad \text{at } r=0 \tag{11}$$

$$u_x=0 \quad \text{at } x=0 \tag{12}$$

where u_r and u_x are the displacements in r and x directions, respectively. And periodic boundary conditions is imposed on line EG to keep its shape under deformation.

A detailed finite element mesh of a typical RVE with a flat fiber tip and interphase is shown in Figure 3, where grid is refined at the end of fiber. The mesh in the regions where high material degradation or high stress concentration is expected to occur is refined. The 4 node quadrilateral axisymmetric element is used in the model. The inhomogeneous interphase is approximated to 20 homogeneous layers in the finite element model, and the Young's modulus of each layer is taken as the average value of the corresponding inhomogeneous layer. It has been checked by comparing with more layers that 20 layers are sufficient to get

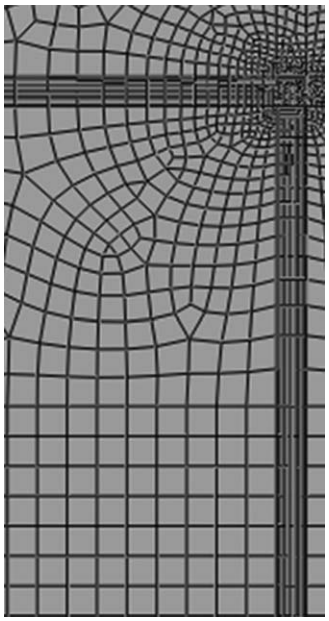

Figure 3. Typical finite element mesh of flat fiber tip.

convergent values when the relative error is set at 1%. Therefore, the assignment of boundary layers at the interface can be regarded as the stress or strain continuity across the interface.[24] The Figure 4 depicts the normal stress values at point *D* to analyze the grid independence. The results show that stress values at point *D* remain unchanged with the total number of elements more than 5473. The grid independence of RVE with other three kinds of fiber tips was also analyzed. The element number used in the analysis is listed in Table I.

RESULTS AND DISCUSSION

Comparison of Stress Distribution by Simulation with that by Shear Lag Model

In order to verify the applicability of the shear lag model to the stress analysis of SFRC with different elastic modulus ratios of the reinforced fiber and rubber matrix, the stress distributions along the direction of the fiber axis ($r = r_f$) of a RVE with flat fiber tip were investigated both by means of the numerical simulation method and the shear lag model. In the analysis process, the elastic modulus ratios (E_f/E_m) are assumed to be 10 and 1000, respectively. The elastic modulus ratio 1000 is corresponding to SFRC, and 10 to metal or resin matrix materials.

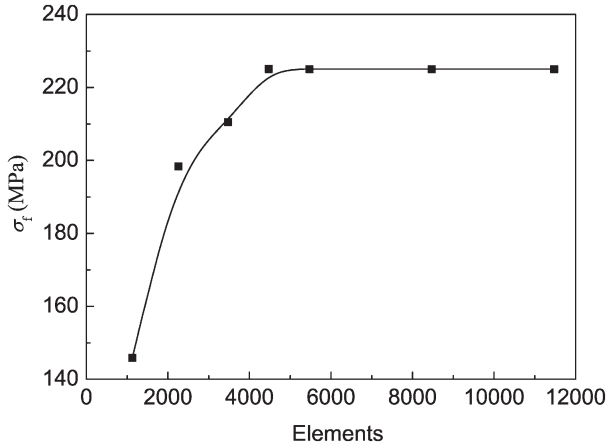

Figure 4. Mesh independence analysis of RVE with a flat fiber tip.

Table I. Elements of Finite Element Models Used in the Analysis

	Flat fiber tip	Semi-elliptical fiber tip	Hemispherical fiber tip	Circular cone fiber tip
Elements	5473	5590	5508	5681

Figure 5 shows the stress distributions at the interface along the direction of the fiber axis. When the $E_f/E_m = 10$, the stress distributions near the end of the fiber occur a small stress concentration. The predicted stress distributions away from the end of the fiber agree well with shear lag model. When the $E_f/E_m = 1000$, the stress distributions near the end of the fiber occur serious stress concentration. The predicted stress distributions over the whole actual fiber length have big errors compared with shear lag model. It can be found that the shear lag model cannot be used to predict the stress distribution in the area of the fiber tip for all fiber reinforced materials and not applicable to the SFRC with large elastic modulus ratio discussed in this article.

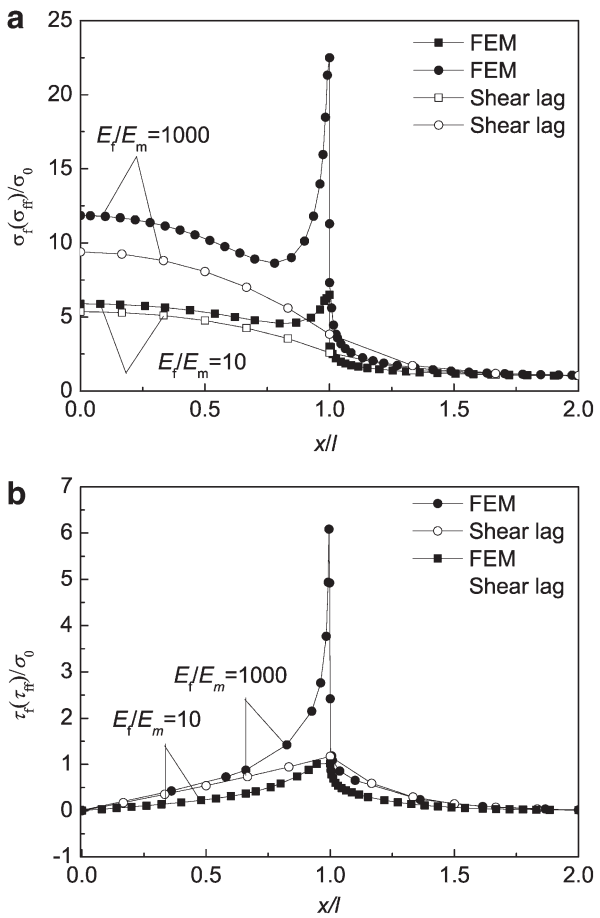

Figure 5. Stress distribution of flat fiber tip along the fiber direction (a) normal stress $\sigma_f(\sigma_{ff})$ and (b) interfacial shear stress $\tau_f(\tau_{ff})$.

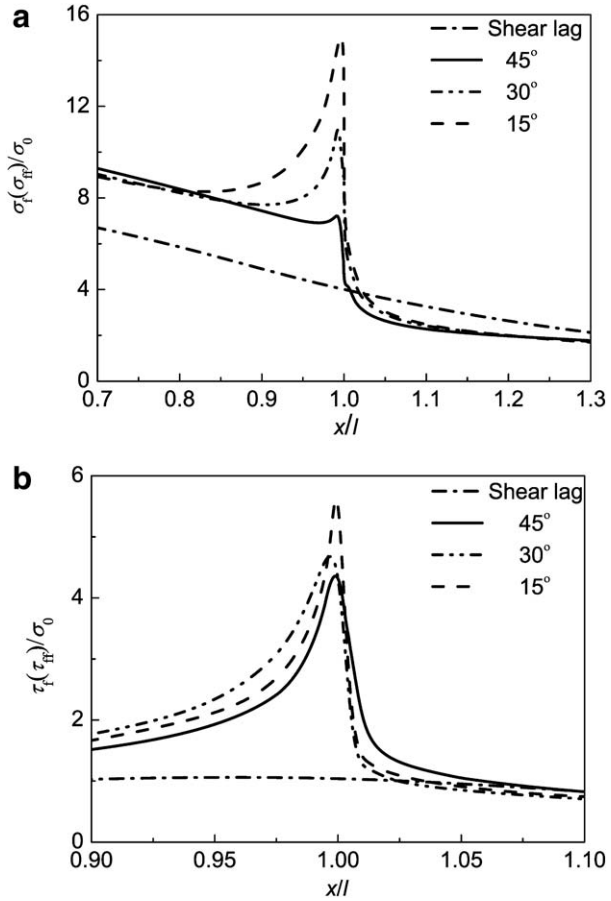

Figure 6. Stress distribution of circular cone fiber tip along the fiber direction (a) normal stress $\sigma_f(\sigma_{ff})$ and (b) interfacial shear stress $\tau_f(\tau_{ff})$.

The Effect of Shapes of Fiber Tip on Stress Distribution

The stress distributions along the fiber direction to the fiber axis ($r = r_f$) of RVE with circular cone fiber tip was illustrated in Figure 6. The normalized fiber normal stress ($\sigma_f(\sigma_{ff})/\sigma_0$) and of normalized fiber coordinate x/l for circular cone fiber tip with $\theta = 45°$, 30°, and 15° are shown in Figure 6(a), and the normalized interfacial shear stress ($\tau_f(\tau_{ff})/\sigma_0$) in Figure 6(b). It can be seen that the stress concentration both of normal stress and interfacial shear stress gradually weakened at the fiber tip with the increase of angle and is the most serious at $\theta = 15°$. The large interfacial shear stress (at $\theta = 15°$) may cause interface deboning failure of SFRC.

Figure 7 illustrates the stress distributions of RVE with semi-ellipsoidal fiber tip along the fiber direction to the fiber axis ($r = r_f$). The normalized fiber normal stress (σ_z/σ_0) of normalized fiber coordinate z/L for semi-ellipsoidal fiber tip with different length-diameter ratios (a/b) are shown in Figure 7(a). The stress concentration occurs at the fiber tip when $a/b = 0.25$. Figure 7(b) reveals that the interfacial shear stress gradually decreases at the fiber tip with the increase of length-diameter ratios. Similarly, the stress concentration occurs at the fiber tip, and it has the maximum value when $a/b = 0.25$.

Figure 8 illustrates the effect of various shapes of fiber tip on the stress distributions, such as flat, circular cone, semi-ellipsoidal, and hemispherical shapes. Figure 8(a) depicts a comparison of normal stresses. Apart from stress intensification, these stress components present steep gradient near the fiber tip depending on its shape. Obviously, the hemispherical fiber tip transfers the normal load with less concentration than the other shapes of fiber tip. The comparison between the interfacial shear stresses is shown in Figure 8(b). The results reveal that the stress concentration of RVE with the hemisphere fiber tip is least among all shapes of the fiber tip, and it is contributed to controlling the interface deboning failure. In all cases, the stress maxima are moved from the corner to the pole position, depending on shapes of fiber tip. The comparison of the current results with shear lag model shows a relative difference in the stress value, and there exit large errors at the fiber tip. The reason is that shear lag model does not take the large modulus ratio (E_f/E_m) and fiber tip geometry into consideration. The stress concentration at the area of the fiber tip is of great importance for the structural integrity of composites reinforced with short fibers. The results presented above indicate that the performances of SFRC depend significantly on the geometrical shape of the fiber tip, and they can be improved by modulating the fiber tip properly.

The Effect of Inhomogeneous Interphase on Stress Distribution

The interfacial adhesion is usually poor between the aramid fiber and rubber matrix, which restricts the mechanical

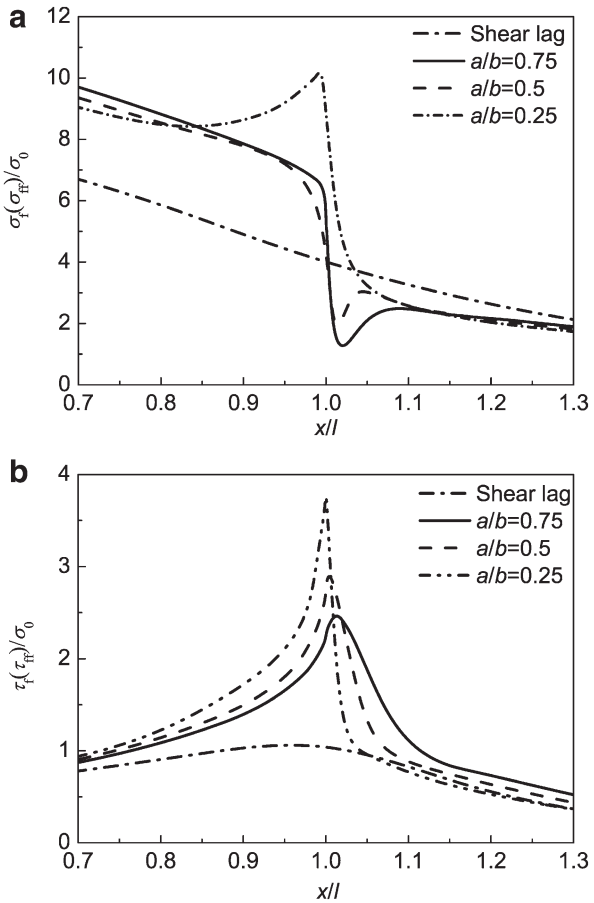

Figure 7. Stress distribution of semi-elliptical fiber tip along the fiber direction (a) normal stress $\sigma_f(\sigma_{ff})$ and (b) interfacial shear stress $\tau_f(\tau_{ff})$.

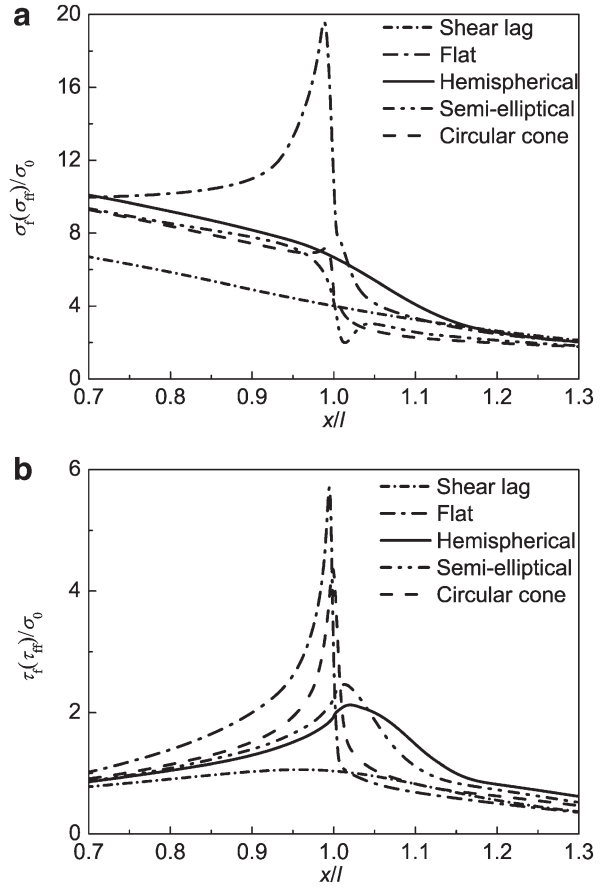

Figure 8. Stress distribution of different shapes of fiber tip along the fiber direction (a) normal stress $\sigma_f(\sigma_{ff})$ and (b) interfacial shear stress $\tau_f(\tau_{ff})$.

properties of the composites, due to a lack of reactive functional groups on the surface and the high crystallinity of the fiber. Epoxy resin coating is an often-used surface treatment method of the aramid fiber.[28–33] Thus, the elastic modulus of interphase varies between 3 GPa (fiber coated with the epoxy resin) and 128 MPa (rubber matrix).

The effects of inhomogeneous interphase property on the comprehensive performances of composites were extensively investigated in the literature.[22–27] As stated by Shen and Li,[24] The inhomogeneous interphase property $P_i(r)$ varied with radius is given as

$$\frac{P_i(r)}{P_{em}} = 1 - D\left[\frac{r_i - r}{r_i - r_f}\right]^Q \quad (13)$$

where P_i is the inhomogeneous interphase properties, such as the elastic modulus (E_i), shear modulus (G_i), Poisson's ratio (v_i), and so on. P_{em} is the equivalent matrix property, r is the radius, the subscripts i and f refer to interface and fiber, respectively. D and Q are material parameters. The parameter D is called an adhesion factor, and $D = [P_{em} - P_i(r_f)]/P_{em}$. The gradient distribution of the inhomogeneous interphase elastic modulus is shown in Figure 9.

In order to investigate the influence of inhomogeneous interphase properties to the stress analysis of SFRC with different interphase elastic moduli and thicknesses, the numerical analysis of the stress distributions both along the direction to the fiber axis ($r = r_f$) and the radial direction in the interphase end (DN as shown in Figure 2) of a RVE with hemispherical fiber tip were conducted.

The normal stress and interfacial shear stress distributions along the direction to the fiber axis ($r = r_f$) for different interphase thicknesses of 0, 0.2, 0.4, and 0.6 μm based on literature[33] were illustrated in Figure 10. When interphase elastic modulus changes along the curve $Q = 1$ in Figure 9, the normal stress increases with the increase of the interphase thickness and interfacial shear stress remains unchanged. Obviously, the normal stress values are higher with interphase than those without interphase.

The effect of interphase elastic moduli on stress distributions with the same interphase thickness (0.2 μm) was also investigated. The results indicate that the normal stress and interfacial shear stress distributions along the direction to the fiber axis remain unchanged with the change of the interphase elastic moduli. This finding is in agreement with the analysis presented by Kiritsi and Anifantis.[25]

The normal and interfacial shear stresses along the radial direction in the interphase end are shown in Figure 11. The results show that the normal stress first increases then decreases when Q value varies from 0.2 to 1, while it first decreases then increases when Q value is in the range of 1–5. The interfacial shear stress decreases with the increase in Q value. It can also be seen that the interfacial shear stress is larger than the normal stress, which reveals the importance of the interfacial layer to the load transfer characteristics. The present results indicate that a significant part of the external load is transferred from the fiber to the matrix through shear stresses within the interphase.

Comparison of FEM Results with Raman Spectroscopy Experimental Data

In Figure 12, there is a comparative graph showing Raman spectroscopy experimental data taken from literature[12] and those obtained by FEM as applied for the case of different shapes fiber tip. In the figure, the points refer to the experimental data for one-half of the fiber. There is a good fit away from the fiber tip, where x/l is less than 0.7. A large scattering of

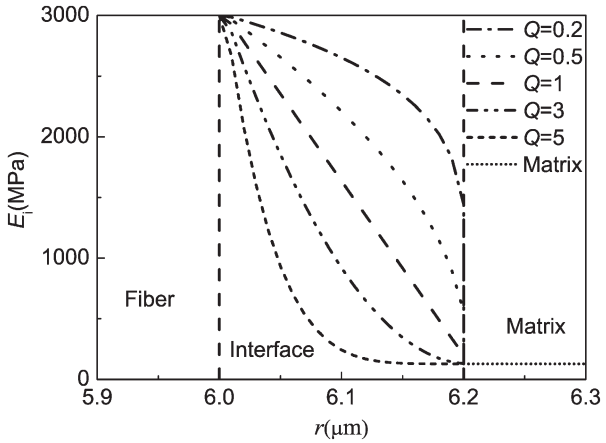

Figure 9. Variation of interphase modulus with Q.

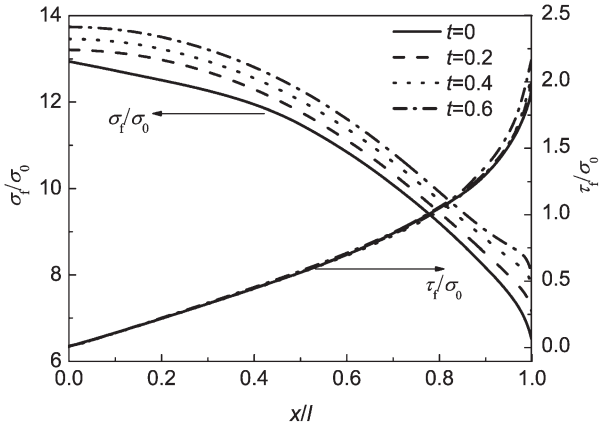

Figure 10. Stress distributions of SFRC with hemispherical fiber tip.

experimental points is obvious near the end of fiber tip ($x/l \geq 0.7$). In this area, the experimental data are less than those obtained by simulation, and the normal stress of flat fiber tip has a severe singularity.

CONCLUSIONS

In the present investigation, the axisymmetric models of RVE of SFRC were established by FEM. The normal and interfacial shear stress distributions along the direction of the fiber axis

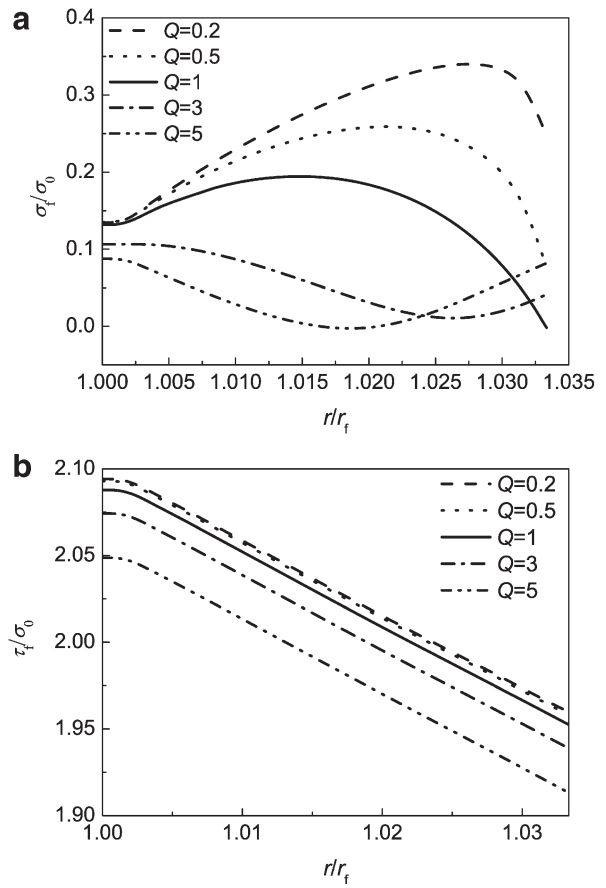

Figure 11. Stress distribution at the location of the fiber tip (a) normal stress σ_f and (b) interfacial shear stress τ_f.

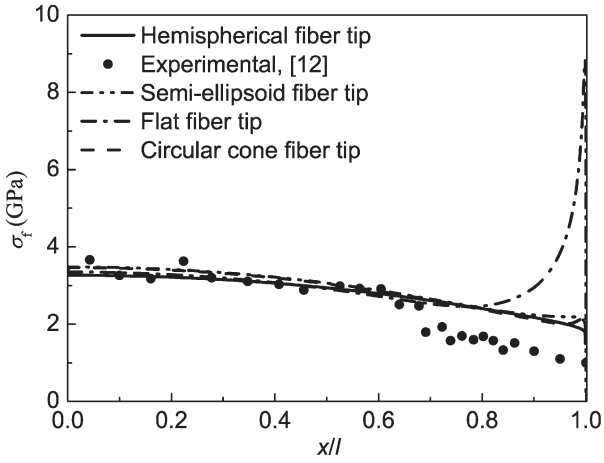

Figure 12. Normal stress distributions by experiment and simulation.

($r = r_f$) with flat fiber tip were investigated both by means of the numerical simulation method and the shear lag model. It was shown that the shear lag model cannot be used to accurately predict the stress distribution in the area of the fiber tip for all fiber reinforced materials and is not applicable to the SFRC with large elastic modulus ratio.

The effect of shapes of fiber tip on the stress distributions of SFRC was investigated. It is found that the hemispherical fiber tip appears the optimum behavior eliminating partly the stress concentrations existing in the case of other shapes of fiber tip. The comparison of the numerical results with those by shear lag model for different shapes of fiber tip was also conducted. It reveals that there is a relative difference in the stress value, and there exit large errors at the fiber tip. The reason is that the large modulus ratio (E_f/E_m) and fiber tip geometry are not taken into consideration in the shear lag model.

Stress distributions with different interphase thicknesses of hemispherical fiber tip of SFRC along the direction to fiber axis were investigated. When $Q = 1$, the normal stress increases with the increase of the interphase thickness and the interfacial shear stress remains unchanged within the scope of the study of the interphase thickness. The normal stress values with interphase are higher than those without interphase.

The effect of interphase elastic moduli on stress distributions was also investigated. The results indicate that either the normal stress or interfacial shear stress distribution along the direction to the fiber axis remains unchanged with the change of the interphase elastic moduli. The stress distributions along the radial direction in the interphase end are largely dependent on the interphase elastic modulus, and the interfacial shear stress is larger than the normal stress. The present results indicate that the interfacial shear stress plays an important role on the external load transfer from the fiber to the matrix.

Numerical results were compared with experimental data derived from Raman spectroscopy. The numerical results and experimental data show a good consistency away from the fiber tip, and there exits a large discrepancy at the location of the fiber tip. The normal stress of flat fiber tip has a severe singularity near the fiber tip.

The results presented in this article indicate that the performances of SFRC depend significantly on the geometrical shape of the fiber tip, and they can be improved by modulating the fiber tip properly. The interphase properties must be taken into account for an accurate prediction of the stress distribution in SFRC.

ACKNOWLEDGMENTS

This project is supported by National Natural Science Foundation of China (Grant No. 51375223) and by Jiangsu Province ordinary university graduate research and innovation (Grant No. CXZZ11_0337).

REFERENCES

1. Gu, B. Q.; Chen, Y.; Zhou, J. F. In Advances in Composite Materials—Ecodesign and Analysis; Attaf, B., Ed.; InTech: Rijeka, Croatia, **2011**.
2. Zhu, D. S.; Gu, B. Q.; Chen, Y. *J. Comput. Theor. Nanosci.* **2008**, *5*, 1546.
3. Gao, X. L.; Li, K. *Int. J. Solids Struct.* **2005**, *42*, 1649.
4. Weber, M. E.; Kamal, M. R. *Polym. Compos.* **2004**, *13*, 133.
5. Cox, H. L. *Br. J. Appl. Phys.* **1952**, *3*, 72.
6. Clyne, T. W. *Mater. Sci. Eng. A* **1989**, *122*, 183.
7. Hsueh, C. H. *J. Mater. Sci.* **1995**, *30*, 219.
8. Nair, S. V.; Kim, H. G. *J. Appl. Mech.* **1992**, *59*, S176.
9. Kim, H. G. *Mater. Sci. Eng. A* **2008**, *483-484*, 135.
10. Starink, M. J.; Syngellakis, S. *Mater. Sci. Eng. A* **1999**, *270*, 270.
11. Jacob, M.; Jose, J.; Jose, S.; Varughese, K. T.; Thomas, S. *J. Appl. Polym. Sci.* **2010**, *117*, 614.
12. Coffey, A. B.; O'Bradaigh, C. M.; Young, R. J. *J. Mater. Sci.* **2007**, *42*, 8053.
13. Lee, D. J.; Oh, H.; Song, Y. S.; Youn, J. R. *Compos. Sci. Technol.* **2012**, *72*, 278.
14. Goutianos, S.; Peijs, T.; Galiotis, C. *Compos. A* **2002**, *33*, 1303.
15. Goutianos, S.; Peijs, T.; Galiotis, C. *Int. J. Solids Struct.* **2002**, *39*, 3217.
16. Stanford, J. L.; Lovell, P. A.; Thongpin, C.; Young, R. J. *Compos. Sci. Technol.* **2000**, *60*, 361.
17. Carlos Afonso, J.; Ranalli, G. *Compos. Sci. Technol.* **2005**, *65*, 1264.
18. Huo, S.; Chevali, V. S.; Ulven, C. A. *J. Appl. Polym. Sci.* **2013**, *128*, 3490.
19. Zhang, B.; Gu, B. Q. In Applied Mechanics and Materials Revealed, Proceedings of 2011 International Conference on Recent Trends in Materials and Mechanical Engineering, Shenzhen, China, January 27–28, Vol. 55; Trans Tech Publications: Germany, **2011**; p 303.
20. Yuan, M. N.; Yang, Y. Q.; Huang, B.; Wu, Y. J. *Rare Metal Mater. Eng.* **2009**, *38*, 1321.
21. Reifsnider, K. L. *Composites* **1994**, *25*, 461.
22. Gao, Z.; Ma, D.; Lv, X.; Zhang, Y. *J. Appl. Polym. Sci.* **2013**, *128*, 1036.
23. Kim, J. K.; Sham, M. L.; Wu, J. *Compos. A* **2001**, *32*, 607.
24. Shen, L.; Li, J. *Int. J. Solids Struct.* **2003**, *40*, 1393.
25. Kiritsi, C. C.; Anifantis, N. K. *Compos. Mater. Sci.* **2001**, *20*, 86.
26. Ngabonziza, Y.; Li, J.; Barry, C. F. *Acta Mech.* **2011**, *220*, 289.
27. Sevostianov, I.; Rodriguez-Ramos, R.; Guinovart-Diaz, R.; Bravo-Castillero, J.; Sabina, F. J. *Int. J. Solids Struct.* **2012**, *49*, 1518.
28. Shirazi, M.; Talma, A. G.; Noordermeer, J. W. M. *J. Appl. Polym. Sci.* **2013**, *128*, 2255.
29. Chattopadhyay, S. K.; Khandal, R. K.; Uppaluri, R.; Ghoshal, A. K. *J. Appl. Polym. Sci.* **2011**, *119*, 1619.
30. Zhang, X.; Chen, P.; Han, D.; Yu, Q.; Ding, Z.; Zhu, X. *Appl. Surf. Sci.* **2013**, *266*, 110.
31. Shi, X.; Nguyen, T. A.; Suo, Z.; Liu, Y.; Avci, R. *Surf. Coat. Technol.* **2009**, *204*, 237.
32. Chen, X.; Zhang, S.; Xu, G.; Zhu, X.; Liu, W. *J. Appl. Polym. Sci.* **2012**, *125*, 1166.
33. Papanicolaou, G. C.; Anifantis, N. K.; Keppas, L. K.; Kosmidou, T. V. *Compos. Interfaces* **2007**, *14*, 131.